Joint Centre for Mesoscale Meteorology, Reading, UK

Mesoscale analysis of arc rainbands in a dry slot

K. A. Browning
N. M. Roberts

Internal Report No. 100

January 1999

Met Office Joint Centre for Mesoscale Meteorology Department of Meteorology
University of Reading PO Box 243 Reading RG6 6BB United Kingdom
Tel: +44 (0)118 931 8425 Fax: +44 (0)118 931 8791
www.metoffice.com

Designed and produced by the Met Office © Crown copyright 2001 01/0240 The Met Office logo is a registered trademark.

Version dated January 99

Mesoscale analysis of arc rainbands in a dry slot

K.A.Browning* and N.M. Roberts
University of Reading

Summary

A series of almost concentric, arc-shaped narrow rainbands was observed travelling at 140 km h^{-1} and producing severe wind gusts over parts of England. Their structure and environment have been analysed using radar and satellite imagery, mesoscale-model diagnostics, surface observations and additional rawinsonde ascents obtained during the Fronts and Atlantic Storms Track Experiment (FASTEX). The multiple-rainband event is shown to have been associated with part of a dry intrusion characterised by a mesoscale vortex/cold pool. The event occurred within the 'dry slot' region of a small frontal cyclone where the mesoscale pool of cold dry air was overunning warm-sector air. Continuous wind profiles from a UHF radar, together with a well-located rawinsonde at the 'epicentre' of the arc rainbands, showed that the major anomaly in the cold pool was an area of locally stronger winds (>40 ms^{-1}) at 800 hPa colocated with the temperature minimum at that level. The observed orientation of the rainbands is explained in terms of the cold frontal structure at this level triggering ascent of the underlying warm moist air. The multiple nature of the arc rainbands remains unexplained; the possibilities of mesoscale gravity waves and conditional symmetric instability are both considered.

* Corresponding author: Joint Centre for Mesoscale Meteorology, Department of Meteorology, University of Reading, P.O. Box 243, Reading, RG6 6BB, UK. (The Joint Centre for Mesoscale Meteorology is supported by the Meteorological Office and by the Department of Meteorology, University of Reading, with funding from the Natural Environment Research Council under the aegis of the Universities Weather Research Network.)

1. Introduction

It has long been recognised that a dry slot is a favoured location for the formation of lines of convective rain : the convective lines form at the leading edge of the dry slot and sometimes within it (eg Carr and Millard 1985). The term dry slot is used in connection with satellite imagery to refer to the relatively cloud-free zone between a major polar-front cloud band and a so-called cloud-head or cloud-hook feature forming on its poleward side in association with a developing extratropical cyclone (Bader et al 1995).

The dry slot marks the leading portion of a dry airstream known as the dry intrusion, which descends from near-tropopause level upstream of the cyclone during cyclogenesis (Young et al 1987, Browning 1997). Where a dry intrusion penetrates into the dry-slot region it is characterised by relatively low wet-bulb potential temperature (θ_w) and it overrides a shallow moist zone of high θ_w The resulting potential instability is often realized as a result of the ascent that normally occurs in this part of a cyclone system. In some situations this leads to lines of deep convective cells, especially over continental regions during warm seasons. In maritime regions such as the British Isles the dry intrusion still triggers convective lines but the convection is often confined to quite shallow layers. Such convective lines can nevertheless produce intense squalls with potentially hazardous gusts. The purpose of this paper is to describe and account for an event of this kind, taking advantage of the rather well defined nature of the particular event and the additional observations available as a result of a special field programme.

The case to be presented occurred in association with a small but vigorous cyclone that crossed the British Isles on 24 February 1997 during the Fronts and Atlantic Storm Track Experiment (FASTEX) (Joly et al 1997). Our attention was drawn to this case by the multiple narrow arc-shaped rainbands that were detected by radar. These rainbands travelled within a dry slot across southern England at 39 m s^{-1}. Parts of the arc rainbands were accompanied by surface

gusts of between 25 and 35 m s^{-1} which caused severe damage in many places. Near the south coast of England this was the major storm event of the January - February FASTEX period.

Such are the exigencies of field programmes that, unlike in the case of other Intensive Observational Periods (IOPs) during FASTEX, we were unable to provide many extra aircraft observations of the precursors to this event over the Atlantic; however, we were able to organize 3-hourly radiosonde ascents from many land-based stations to supplement the already good operational coverage available in this region from surface stations and radars. Accordingly this event was given the label IOP 18A. In this study we examine the arc rainbands observed in IOP 18A using a combination of direct observations and NWP products from the Limited Area and mesoscale versions of the operational Met Office Unified Model (Cullen 1993). The operational model runs were able to benefit from the assimilation of data from the extra radiosonde ascents that were fed in near-real time into the Global Telecommunications System (GTS) as part of FASTEX.

The results of the case study are given in Sections 2 to 5. Section 2 presents the synoptic context, Section 3 describes the structure of the arc rainbands and Sections 4 and 5 analyse the thermodynamic structure of the dry-slot region where the arc rainbands occurred. There were several such rainbands spaced 50 to 100 km apart and they seemed to have an epicentre that travelled along the English Channel. Their appearance was suggestive of phenomena related to inertia-gravity waves, or so-called mesoscale gravity waves, about which there is a large literature (eg Uccellini and Koch 1987, Powers and Reed 1993). In a recent study by Trexler et al (1997) an arc-shaped convective rainband observed within a dry slot was shown to be related to such waves. The present case, however, was not associated with the rather large surface pressure perturbations found in most studies of mesoscale gravity waves. Nor, as we shall show, did it strongly satisfy all of the criteria for the maintenance of such waves. These issues are discussed in Section 6.

2. Synoptic context

The phenomena analysed in this study were associated with a small frontal cyclone that crossed Wales and England during the evening of 24 February 1997. The cyclone is labelled LZ in the operational Met Office surface analyses for 1200 UTC, 24 February and 0000 UTC, 25 February, shown in Figs. 1 (a) and (b) respectively. Although the cyclone developed only a small closed circulation, it produced heavy rain and gale-force gusts. The dry intrusion associated with the cyclone shows up in the water vapour imagery (Fig 2) as a dark zone which darkened and expanded with time as it approached southern Britain. The earlier history of the dry intrusion (not shown) could be traced back to 1500 UTC on 23 February, at which time the dark zone was passing over Newfoundland. By 1830 UTC on 24 February, Fig. 2(c) shows the dry intrusion as a dry slot sandwiched between what is confirmed by infrared imagery to be a cloud head over northern England and a polar-front cloud band extending west-to-east along the English Channel and southern England. As shown later, the region of dry air responsible for the dry slot actually undercut the high-level cloud of the polar-front cloud band such that the southern boundary of the dry air extended about 200 km south of the observed dry slot.

3. The observed structure and effects of the arc rainbands

The arc rainbands occurred beneath the dry intrusion, both in the dry-slot region and to some extent where the dry intrusion went underneath the edge of the polar-front cloud-band. The associated cloud tops extended up to about -20°C (500 hPa) at their highest, but they were mainly below this (at least where they were visible).

The arc rainbands were best observed using the weather radar network. The radar signature of individual rainbands was in some ways reminiscent of Fujita's (1978) 'bow echoes', whose primary significance is their association with severe surface wind gusts. Viewed in action replay the echoes in the present

Fig.1

(a)

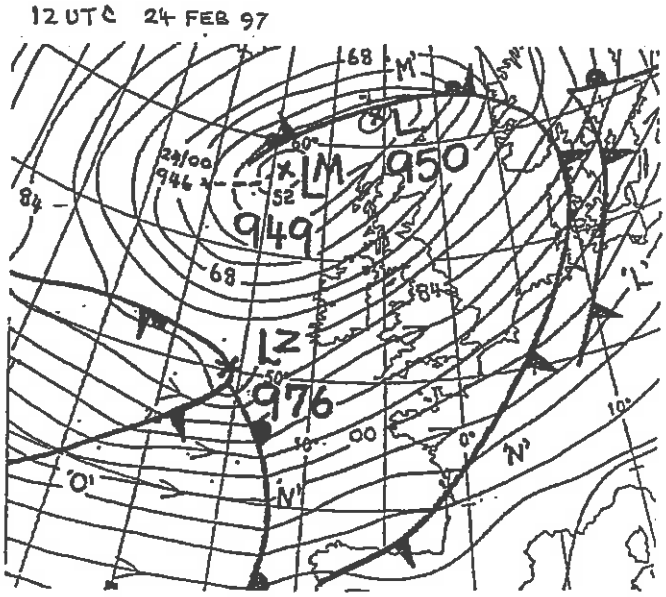

(b)

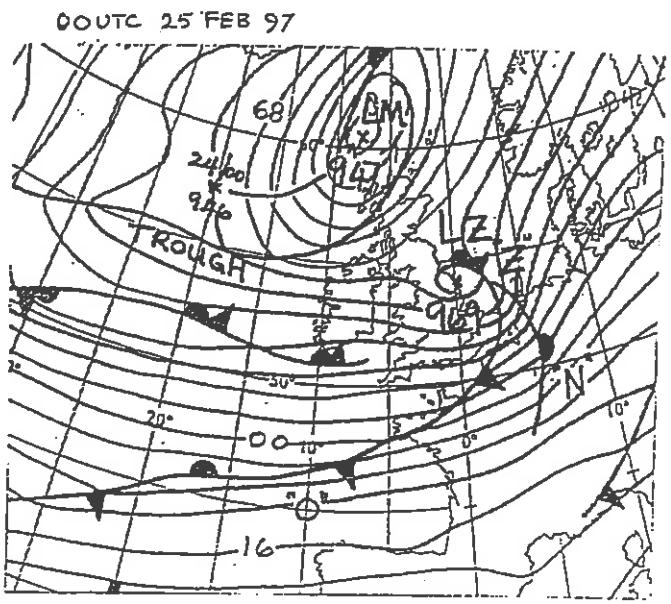

Fig. 1 Operational surface analyses from the UK Met Office for (a) 1200 UTC, 24 February and (b) 0000 UTC, 25 February 1997.

Fig. 2

(a) (b) (c)

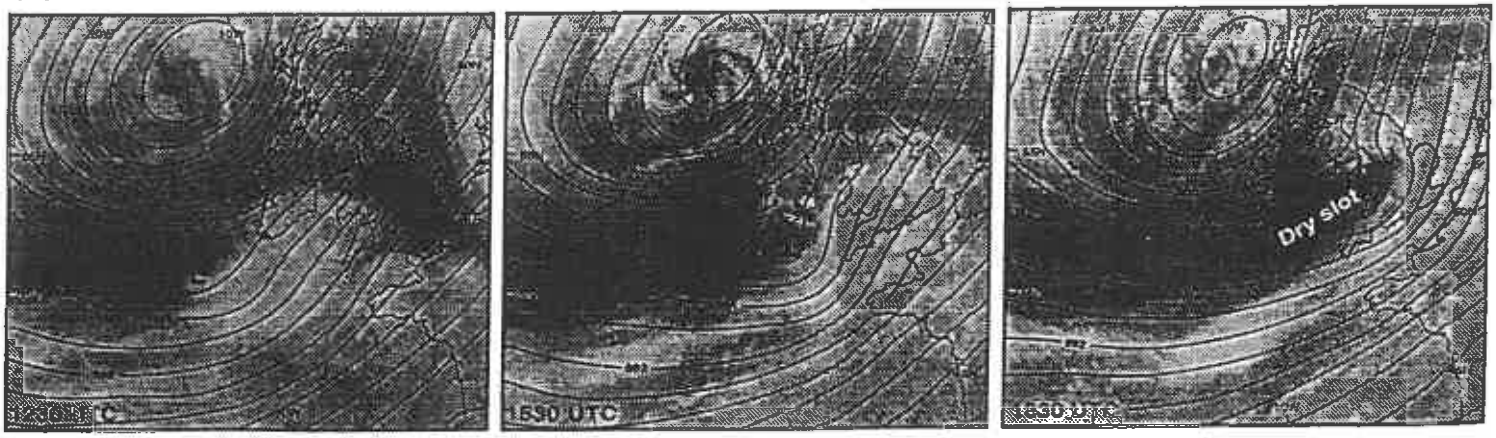

Fig. 2 Meteosat water vapour images at (a) 1230, (b) 1530 and (c) 1830 UTC, 24 February 1997, showing the dry intrusion (dark zone) intruding into the cloud area during the development of the cloud head (seen to the north of the dry slot at 1830 UTC in (c)). Also shown are corresponding Limited Area model analyses (a and c) and the (T+3) forecast (b) of the mean-sea-level pressure. L marks the position of the associated surface low during the development of its closed circulation.

case are seen as a series of initially almost concentric arcs emanating from an 'epicentre' that travelled along the English Channel close to the south coast of England. Their behaviour is summarized in Fig 3.

The 1830 UTC radar rainfall display in Fig 3(a) shows a large area of widespread continuous warm frontal rain travelling away toward the east, with a ragged rear edge extending from south Wales to northwest France. The ragged rear edge of the continuous rain coincided with the arrival of the dry-intrusion air at middle levels. Beneath the dry intrusion there were five arc rainbands highlighted by thin black lines in Fig. 3(a). Although not convincing on the basis of single pictures, because of gaps in different parts of the rainbands at any given time, this analysis is more credible when the radar network pictures are viewed as a full sequence. Two hours later the five rainbands can still be seen (Fig.3(b)) as they sped across southern England at a velocity of 39 ms^{-1} (140 km h^{-1}) from 257°.

The tracings in Figs. 3(c) and (d) show successive positions of three of the rainbands (R2, R3 and R5) and also the locations of stations, autographic records from which are reproduced in Figs. 4 and 5. Location L (RAF Lyneham) in Fig. 3(c) was affected by Rainband R2 which passed Lyneham twice. The first passage was at 1930 UTC when the leading edge, orientated northwest-southeast (NW-SE), passed overhead. The second passage was at 2030 UTC when the trailing part of R2, orientated SW-NE, passed overhead. The surface wind records for Lyneham are shown in Fig 4. There was no surface signature during the first passage, but during the second passage there was a 30-deg veer and a strengthening of the wind, with gusts to 56 knots (28 ms^{-1}). Autographic temperature records were not available for Lyneham.

Location O (RAF Odiham) in Fig. 3(d) was affected by Rainband R3. The leading portion of the trailing part of the rainband passed overhead just after 2030 UTC. The trailing part of the rainband then remained overhead, travelling along its own length, until some time after 2130 UTC. The autographic wind

Fig.4

24 February 1997 Lyneham

(a)

(b)

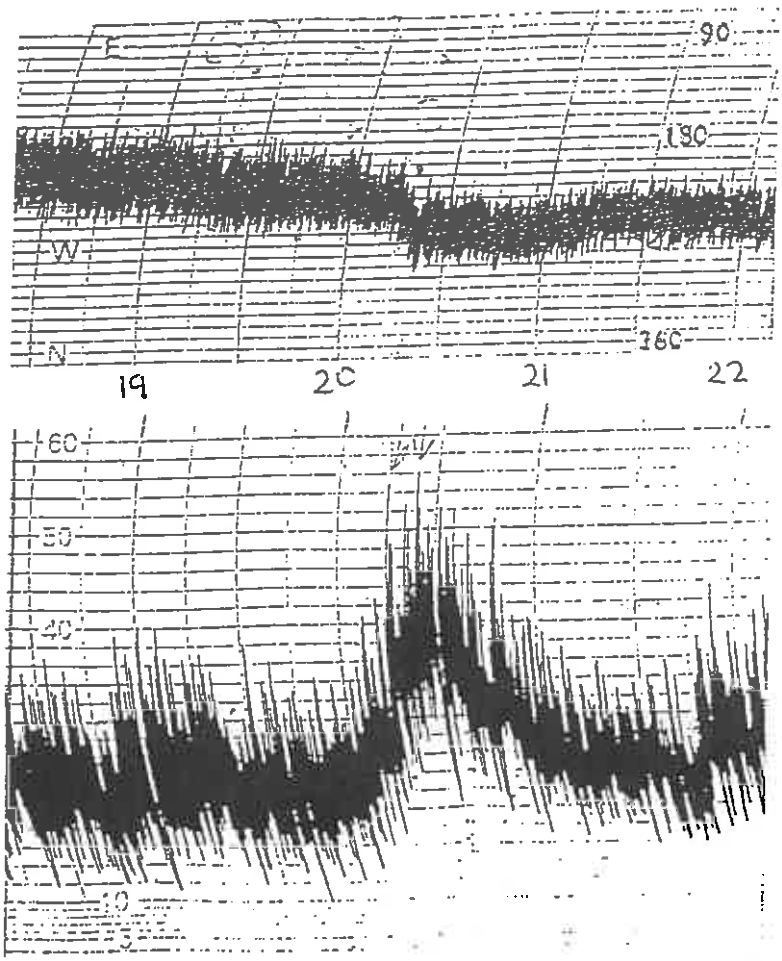

Fig. 4. Autographic wind record from RAF Lyneham from, 1830 to 2200 UTC, 24 February 1997. (a): wind direction. (b): wind speed. The location of Lyneham (L) is marked on Fig. 3(c).

Fig.5

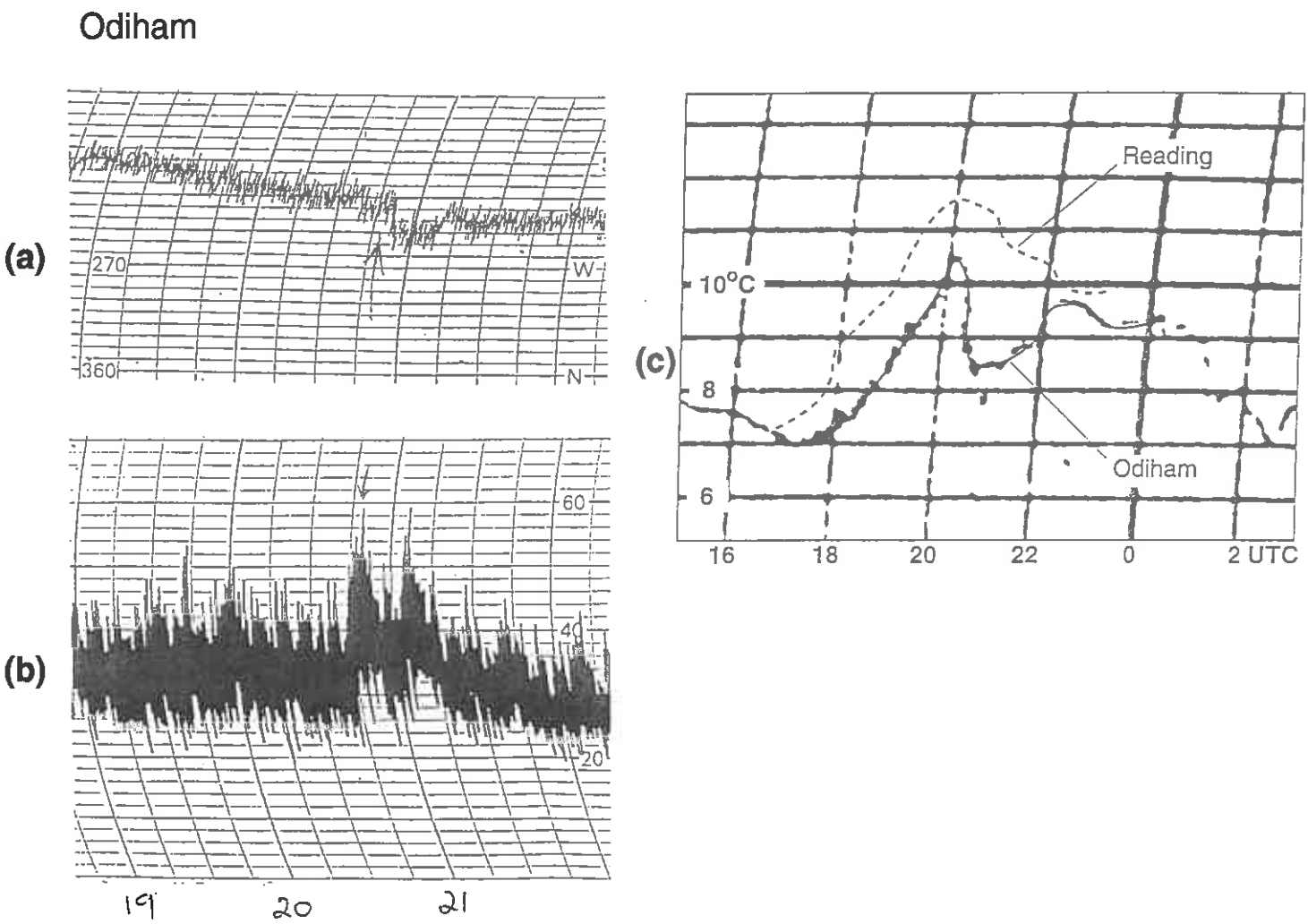

Fig. 5. Autographic records from RAF Odiham and Univ. of Reading (at locations O and R in Fig.3d). (a) and (b) : wind direction and speed at Odiham. (c) : temperature at Odiham (solid line), with the time-adjusted Reading temperature trace superimposed (dashed line).

traces from RAF Odiham (Fig.5(a) and (b)) show a 25-deg veer and the first of two 59 knot (29 ms^{-1}) gusts at 2040 UTC, just after the arrival of the rainband. This was accompanied by a 2°C drop in temperature (Fig.5(c)). The temperature remained low throughout the period the trailing rainband was overhead and then recovered as the rainband moved away after 2200 UTC. The rainbands were convective (see later) and it is reasonable to assume that the local reductions in θ_w were due to downdraughts. The temperature record from a station (Reading) a few kilometres north of the track of this rainband (superimposed on Fig.5(c) with appropriate time adjustment), shows that the cold burst during the passage of the rainband occurred during the otherwise warm period. Pressure jumps associated with the passage of the cold outflow were no more than 0.5 hPa at Odiham and generally even less elsewhere.

A similar analysis of other autographic records has been carried out and then combined with hourly reports from synoptic observing stations and weather radar observations to provide hourly surface mesoanalyses of the distribution of wet-bulb potential temperature (θ_w). One of these, for 2100 UTC, is shown in Fig. 6. Individual observations are plotted; lines of observations represent the locations of 5-min readings from autographic records converted from time to space according to a system velocity of 140 km h^{-1} from 257°. The regions of heaviest rain (coloured red) associated with the two most intense arc rainbands (dotted lines labelled R2 and R3) are seen to occur within the wedge of high-θ_w air at the surface corresponding to the warm sector. These parts of the rainbands are depicted in Fig 6 as producing a localized reduction in θ_w. Observational evidence for this was shown in Fig.5(c) for one of the rainbands and, in the absence of well placed observations, a similar behaviour is assumed for the other intense rainbands.

The cold outflows associated with the parts of the arc rainbands within the warm sector are where most of the severe surface gusts occurred. Not all parts of the arc rainbands produced surface gusts; for example, we showed earlier that the leading part of arc rainband R2 produced no such effects as it passed over

Lyneham. This was probably because this part of the rainband was situated ahead of the surface warm front which would have made it difficult for any cold downdraughts to penetrate to the surface. (The situation was further complicated in this case study by the fact that not all of the severe gusts were associated with active rainbands. In particular, an area of gusts in the East Midlands occurred in the absence of precipitation, in a part of Rainband R1 that had decayed during the previous hour. This decay coincided with the arrival of a small pocket of dry air which ran ahead of the main dry intrusion at 800 hPa into the region just south of the cyclone centre, close to the northern-most tip of the 10.5° C isopleth.)

4. The thermodynamic structure as determined from the mesoscale model

The detailed structure of the region where the arc rainbands were occurring is well revealed by the mesoscale version of the operational Unified Model (0.15 x 0.15°, 31 levels, 92 x 92 points encompassing the British Isles, rotated pole at 37.5°N, 177.5°E. See appendix of Browning et al (1997) for more details and further references). Figures 7, 8 and 9 show the model analysis for 1800 UTC, on 24 February 1997. This analysis benefits from assimilation of 3-hourly ascents from many radiosondes; those from Valentia (in southwest Ireland), Aberporth (west Wales), Camborne and Herstmonceux (southern England) and Brest (northwest France) are likely to have been particularly beneficial.

Figure 7 shows key aspects of the structure in plan view at a time when the rainbands were centred over Camborne (C) in extreme southwest England (see Fig.3(a)). The location C was in the exit region of a strong upper-level jet (see 300 hPa isotachs, dashed lines). A dry intrusion was present at middle levels (dotted curve shows leading edge of dry air at 600 hPa). It was characterised by low wet-bulb potential temperature (θ_w) (thin solid lines show θ_w at 600 hPa). This was overrunning a region of high θ_w at low levels (thick solid line shows warm sector defined by θ_w = 12.5°C at 900 hPa).The mid-level, low- θ_w anomaly over southwest England extended down to 800 hPa and it was at this level that the

Fig.7

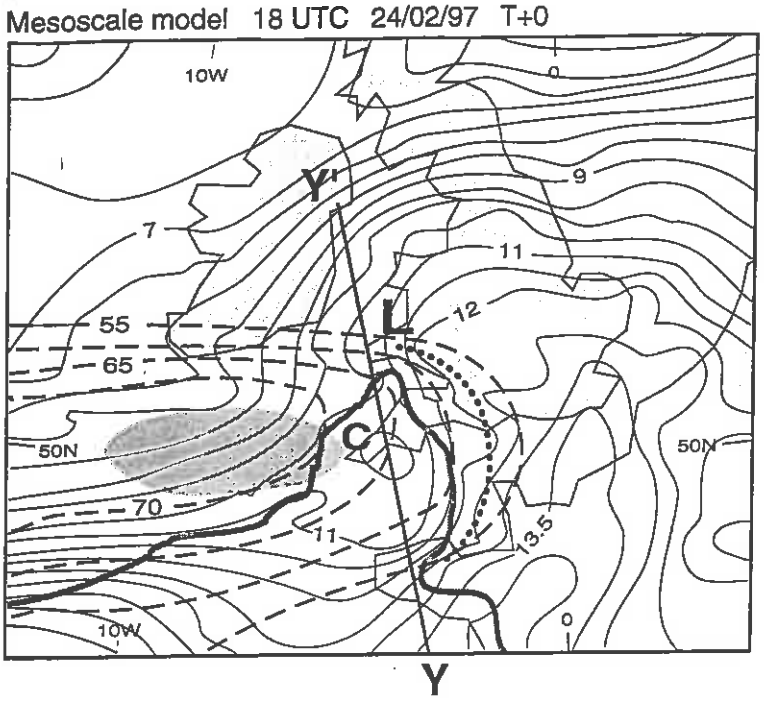

Fig. 7. Mesoscale model analysis for 1800 UTC, 24 February 1997, showing wind speed at 300 hPa (dashed lines at 5 m s $^{-1}$ intervals above 55 m s^{-1}), wet-bulb potential temperature at 600 hPa (thin solid lines at 0.5 deg C intervals), the leading edge of the dry air (RH <70%) at 600 hPa (dotted line) and the warm sector delineated by the 12.5 deg C θ_w-contour at 900 hPa (thick solid line). L marks the position of the surface low. C marks the location of Camborne and YY' denotes the position of the cross-section in Fig.9. The shaded area just west of C denotes a region of intense slantwise convective available potential energy (>500 J kg^{-1}).

Fig.8

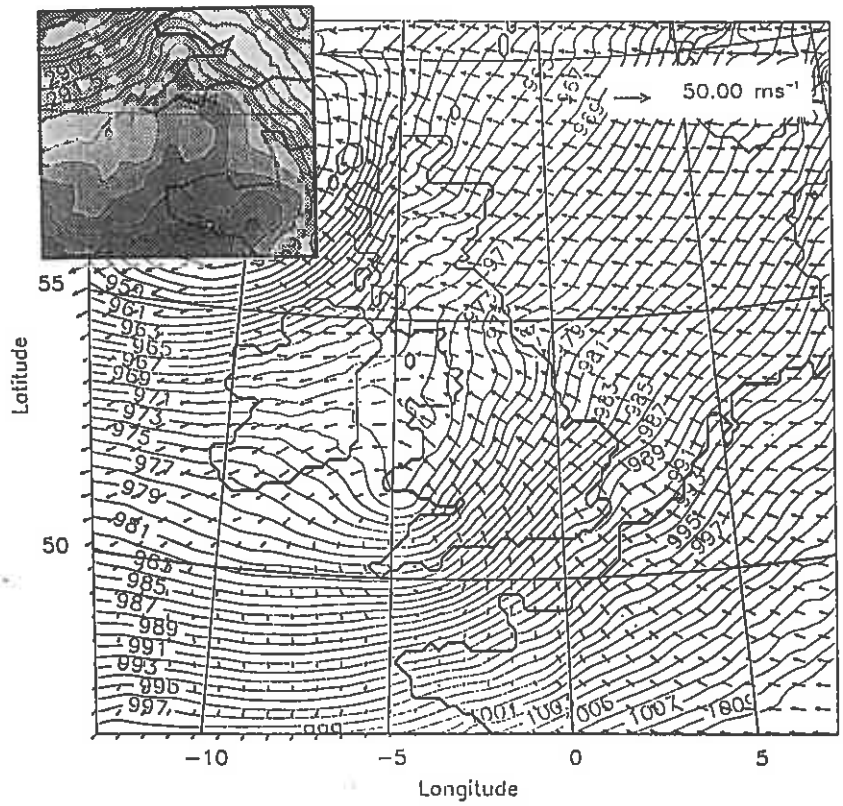

Fig. 8. Mesoscale model analysis for 1800 UTC, 24 February 1997, showing system relative winds at 800 hPa superimposed on mean-sea-level pressure (isobars at 1hPa intervals) The insert shows the distribution of dry-bulb potential temperature at 800 hPa for a small sub-area around Camborne (isopleths at 0.5°C intervals, with areas warmer and colder than 291-292°C shaded more darkly).

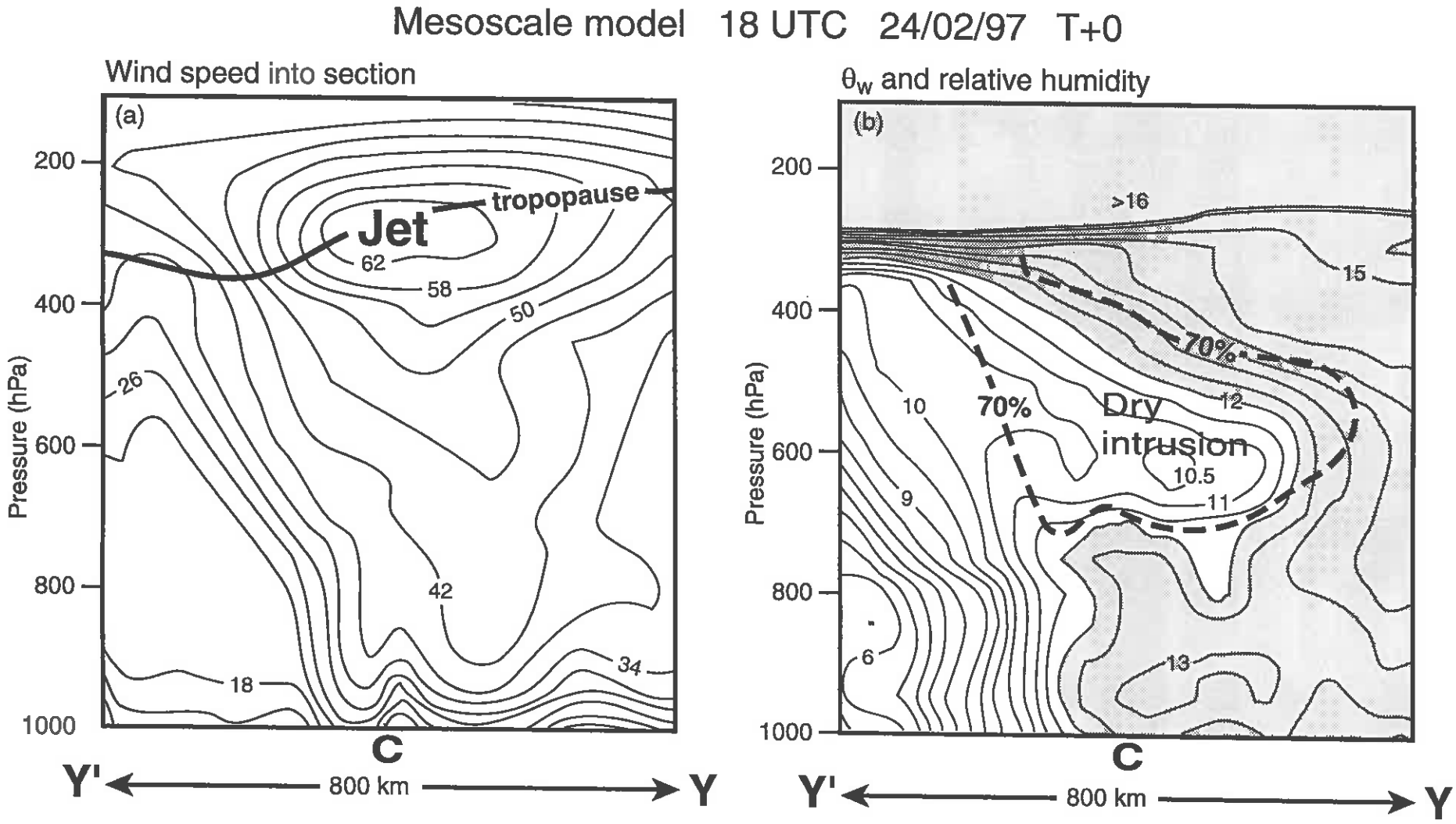

Fig. 9. Vertical section through the centre of the mesoscale vortex/cold pool, normal to its direction of travel, at 1800 UTC, 24 February 1997, as derived from the mesoscale model. See Fig.7 for position of section (YY'). (a) Wind component perpendicular to the section (isotachs at 4 m s^{-1} intervals). Also shown is the model's tropopause (2 PV units) (thick solid line). (b) Wet-bulb potential temperature (isopleths at 0.5°C intervals, with areas warmer than 12°C shaded). The dashed line shows the intrusion of dry air (RH < 70%).

Fig.9

associated θ- anomaly was best observed: see the incursion of relatively cold air from the west into the warm tongue south of Devon in the inset to Fig.8. The accompanying mesoscale vortex, as evidenced in the system-relative wind pattern, is shown in the main part of Fig.8.

A model-derived cross-section through the middle-level mesoscale vortex/cold pool, perpendicular to its direction of travel, is shown in Fig. 9. This section is located along the line YY' in Fig.7. Figure 9(a) shows that the region of the rainbands near the centre of the vortex (near C) was beneath the axis of the jet (in its exit region). The θ_w-pattern in Fig.9(b) shows that the low-θ_w air in this region, associated with the dry intrusion (70% relative-humidity contour shown dashed), was overunning high -θ_w air in the lower troposphere and giving rise to potential instability ,especially above 800 hPa. However, the instability that was mostly responsible for the convective rainbands was that occurring between 900 and 800 hPa. This tended to be underestimated by the model and is better revealed by the direct observations, as shown in section 5.

5. UHF radar and radiosonde observations during the passage of the arc rainbands and mesoscale cold vortex.

Figures 10(a and b) show time-height sections based on nominally 3-hourly rawinsondes and continuous UHF radar profiles at Camborne, which was close to the epicentre of the arc rainbands at 1800 UTC. The sections are approximately equivalent to sections through C at right-angles to YY' in Fig.7. Each hour on the time scale corresponds to a distance of 140 km, at least for features in and generated by the cold air mass.

Figure 10(a) shows subjectively analysed contours of wet-bulb potential temperature (θ_w) obtained from the rawinsondes superimposed on the echo power received from the vertically pointing UHF radar. There are two factors contributing to the echo power received by a UHF radar (eg Gage et al 1994). The first is Bragg scattering from refractive index inhomogeneities owing to

turbulent mixing of temperature and humidity gradients, especially within the boundary layer. This accounts for much of the signal detected in the lowest kilometer or so, especially before 1320 UTC and after 1800 UTC. The second factor is Rayleigh scattering from precipitation particles, especially during the period of widespread frontal precipitation, from 1320 UTC until the arrival of the surface warm front at 1710 UTC, and also during periods of deeper convection leading to the columns of echo which extended up to between 3 and 6 km. Some of these columnar echoes can be identified with the passage of rainbands R1 – R4. An analysis of the echo power and the radar-derived vertical velocity of the precipitation particles, has also enabled the height of the melting layer (bright band) to be obtained between 1330 and 1550 UTC (dashed line in Fig.10(a)) and this has helped in the drawing of the θ_w- isopleths during this period (no bright band was detectable at other times).

A shallow layer of warm moist air with $\theta_w \geq 12^0$C, which can be interpreted as a warm conveyor belt, can be seen in Fig 10 (a) to be situated above the strong warm-frontal zone. The warm conveyor belt is itself being overrun by dry-intrusion air with low θ_w as in the split-front model of Browning and Monk (1982). The overrunning is very substantial: the leading edge of the dry intrusion (at 1500 UTC) is as much as 4½ hours in advance of the passage of the surface cold front. The value of θ_w can be seen to decrease progressively with time (distance) within the dry intrusion and the convective arc rainbands were clearly associated with the overunning of this low-θ_w air. The first (unnumbered) rainbands passed before 1700 UTC. Four of the arc rainbands then followed between 1730 and 1930 UTC (the fifth passed just to the south of Camborne). It is possible that θ_w decreased in a series of steps corresponding to the passage of each rainband but this is not resolvable from the widely-spaced radiosondes. There is, however, evidence from the continuous UHF radar wind measurements (Fig.10(b)) for a series of wind pulses corresponding to tilted layers of convergence/divergence (and hence slantwise ascent/descent). These were spaced at intervals corresponding approximately to the spacing of the arc rainbands. Each of these may have been associated with a mesoscale upper-level cold front but it is not possible to prove

this with the available observations. The amplitude of the pulses is typically 5 m s $^{-1}$ and the spacing is typically rather less than 100 km (corresponding to a period of about ½ hour).

Parts of the arc rainbands developed cloud tops up to 500 hPa as they travelled across England but, at the time they passed over Camborne, Fig.10(a) shows that the tops were mostly near 650 hPa. The very dry air of the dry intrusion was restricted to the layer close to and above the level of the cloud tops, but there is evidence of the intrusion of layers of low-θ_w air at lower levels : see, for example, the feature labelled 'Low-θ_w' in the sounding in Fig.11, which was close to rainband R3. A similar layer of low θ_w could be seen close to rainband R4 in the 2000 UTC sounding (not shown). These layers are believed to have been the major cause of the convection that led to the arc rainbands. Moreover, once the convective rainbands had been triggered, evaporation and melting within these low-θ_w and initially sub-saturated layers is likely to have led to further cooling and destabilization

We shall now consider these low-level incursions of low -θ_w air and the associated potential instability in more detail. Unfortunately, even with soundings nominally every 3 hours, their spacing is still so large that it is difficult to analyse the θ_w pattern in Fig.10(a) unambiguously. A particular problem is how to account for the pockets of low -θ_w air that were observed at low levels (eg at 800 hPa in the radiosonde ascent at 1800 UTC): it is not immediately obvious whether to draw the θ_w contours at low levels sloping down from left to right or, instead, to draw them sloping down from right to left as we have in fact done in Fig. 10(a). Putting it another way, we know that the low -θ_w air was overtaking the rainbands at middle levels, but did the pockets of low -θ_w air accomplish their final descent to very low levels via descent from the left (ie while still overtaking the system) or from the right (ie by decelerating and then travelling more slowly than the system)? One factor that has guided us in the drawing of the θ_w- isopleths in Fig.10(a) is the slope of the top of the boundary layer as inferred from the echo top after the passage of the surface warm front. For example, between 2200 and

2000 UTC the boundary-layer top can be inferred (from the upper envelope of the shallow convective echoes) to slope upwards from left to right ; the top then drops down from 2 to 1 km with some evidence that it rises to 2 km again just to the right of the penetrative convection associated with rainband R4, before dropping back down to 1km between 1800 and 1900 UTC. This constrains the θ_w- isopleths to be drawn sloping up to the right such that the layers of low -θ_w air that show up between 1 and 2 km in the radiosondes at 1800 and 2000 UTC would have had to have been fed by dry low -θ_w air approaching in a system-relative sense from the right (east). The shallow layers of high -θ_w layers air situated just above these low -θ_w layers may have been due to slantwise ascent above the descending low -θ_w air and/or to air detrained from the penetrative convection responsible for the arc rainbands.

Figure 11 shows that the speed of the wind at the level of the low-θ_w layer at 800 hPa was close to the speed of the rainbands. However, it is significant that the windspeed at 800 hPa was also a minimum (40 ms^{-1}. compared with 41 m s^{-1} at 850 hPa and 43 m s^{-1} at 750 hPa). Although it could be argued that, the magnitude of this minimum is too small to be significant, we speculate that, because of the difficulty in resolving such features from standard radiosonde ascents, the minimum windspeed could in reality have been significantly less than 40 ms^{-1}. This speculation is upheld by the profiler winds in Fig.10(b) where a layer of relatively weak winds (yellow <37.5 ms^{-1}) is seen descending from 1500m at 1800 UTC to 800m at 1850UTC. The axis of this wind minimum coincides with the axis of the layer of low θ_w drawn in Fig. 10(a) . Even lower wind speeds (blue shading in Fig.10(b) are associated with the other layers of low -θ_w air shown descending between 1930 and 2000 UTC (Fig. 10 (a)). In summary, therefore the winds are consistent with the way in which the θ_w – contours in Fig.10(a) have been drawn, implying that the dry layers of low θ_w were penetrating rearwards relative to the fast-moving flow above them. The rearward penetration drawn in Fig.10(a) is about 140 km. Assuming a 3 ms^{-1} rearward relative flow, it would have taken on the order of 12 hours for the air to have penetrated this distance, which is not inconsistent with the lifetime of the system.

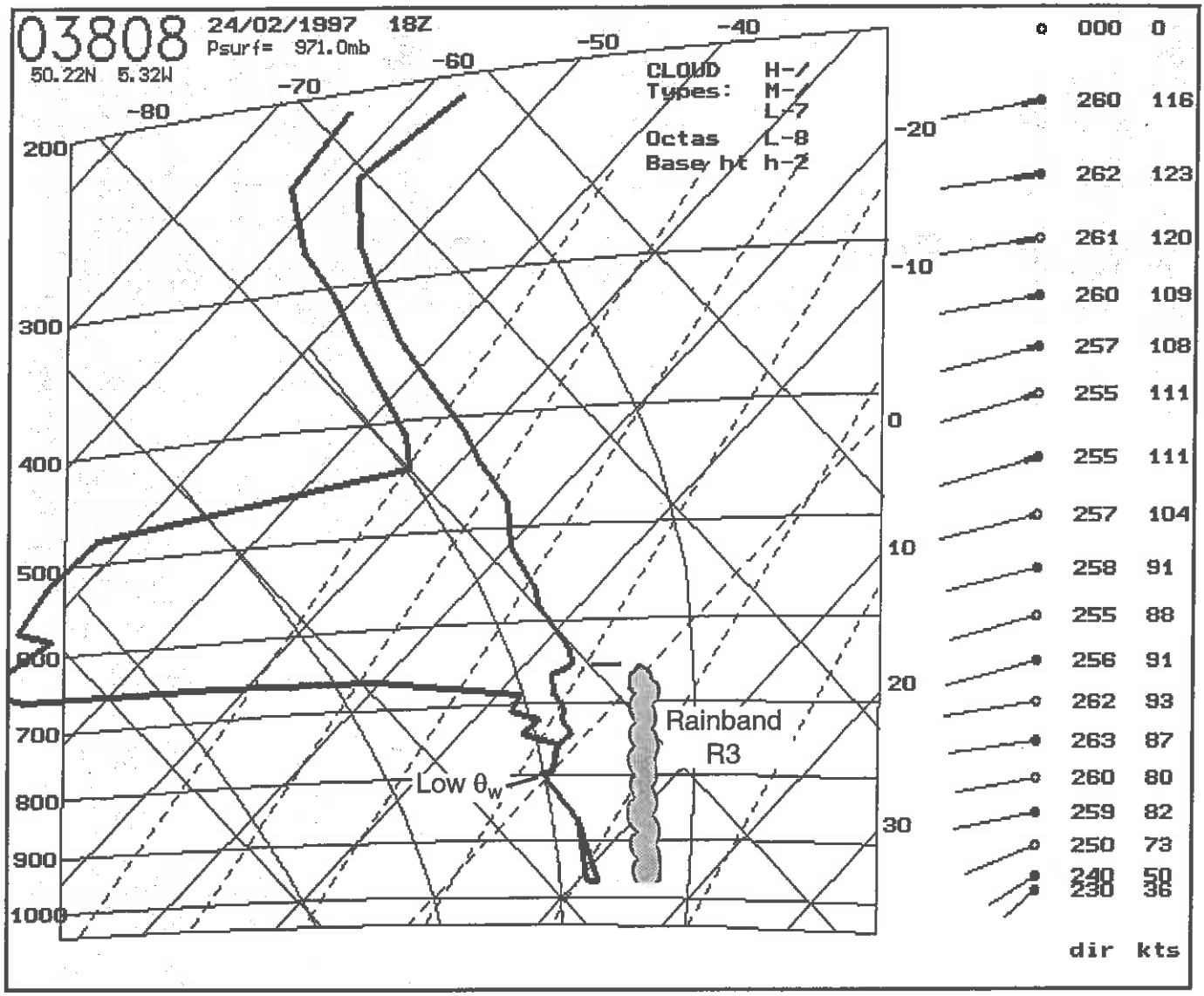

Fig. 11. Sounding at 1800 UTC, 24 February 1997, at Camborne (50.22°N, 5.32°W, at location C in Fig. 7). Solid lines show temperature and dew point. The main dry intrusion with low θ_w is between 680 and 450 hPa. The apparently saturated layer with a dry-adiabatic lapse rate below 800 hPa may in some respects be an artefact due to wetting of the temperature sensor but nevertheless it is believed that there was a significant θ_w- minimum at 800 hPa. This layer, labelled low θ_w, is thought to have been responsible for convective rainband R3 whose vertical extent is sketched. Wind speeds shown at the right are in knots.

Fig.11

6. Synthesis and discussion

The rainbands in this case study were observed to be:

- long (100s of km)
- narrow (10 km)
- convective
- not very deep (tops to between 700 and 500 hPa)
- arc shaped
- rather periodic (not-quite concentric arcs with spacing of order 100 km)
- rapidly moving (140km h^{-1} from 257°)

X

The rainbands may be analysed as upper cold fronts (strictly mid-tropospheric cold θ_w-fronts) as shown in Fig.12, which is based in detail on the analysis in Fig.6.The upper cold fronts were embedded within a broad cold-frontal zone associated with the advancing dry intrusion. The dry- intrusion air was characterised by westerly winds within ± 3 m s^{-1} of the velocity of the rainbands. Within this flow, the UHF radar evidence in Fig.10(b) reveals a series of wind pulses (amplitude 5 m s^{-1} and horizontal spacing < 100 km) which show a degree of continuity in the vertical and are sloping downwards from front to rear. The pulses are believed to have corresponded to a series of mid-level mesoscale cold fronts similar to those observed by Kreitzberg (1968). As in the study of Locatelli et al (1997) the cold fronts aloft produced surface pressure perturbations of only a fraction of a millibar (hPa) yet they were able to trigger convective rainbands. As the mesoscale cold fronts overran the warm conveyor belt, the resulting convection of air originating in the warm conveyor belt gradually eroded and thinned the associated layer of high -θ_w air. The extent to which the wind pulses attributed to upper-level cold fronts were themselves enhanced by the convection is not clear

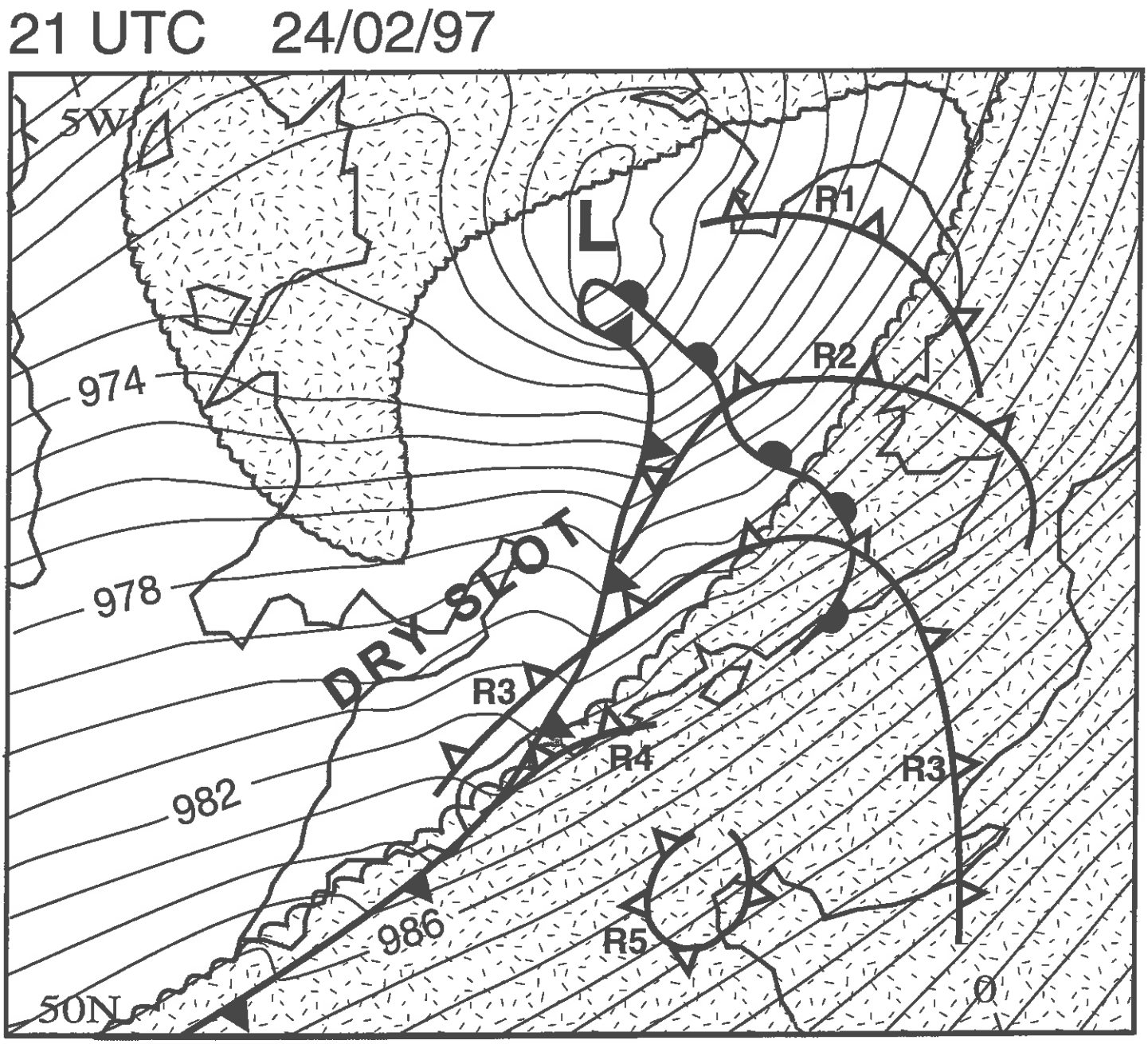

Fig.12. Surface and frontal analysis for 2100 UTC, 24 February 1997. Isobars are at 1-hPa intervals. Surface warm and cold fronts are plotted conventionally. Upper cold fronts associated with the arc rainbands are shown with open symbols. The stippled area is added to show the extent of the cloud above the –15°C level. The dry intrusion air also extends south of the labelled dry-slot region beneath the polar-front cloud over the English Channel and south-east England.

Fig.12

The strongest convection (eg parts of rainbands R2 and R3) occurred where the upper cold fronts were overunning the warm conveyor belt while it was still in contact with the ground (ie in the warm sector). At Camborne the main arc rainbands passed overhead between 1730 and 1930 UTC when the strong westerlies of the dry intrusion were penetrating to their lowest level directly above the warm sector (Fig.10(b)). Figure 11 shows that the θ_w at the surface exceeded θ_w at 800 mb by 2 to 3°C and convection occurred to 700 mb. Two or three hours later in the same relative location, the convection became more intense, with very heavy rain and cold downdraughts that penetrated to the surface causing severe wind gusts. Parts of the arc rainbands ahead of the surface warm front would have been unable to produce downdraughts capable of penetrating to the surface through the cold near-surface air.

We think we broadly understand the nature and origin of the arc rainbands, but the question remains as to the reason for the quasi-periodic series of wind pulses within the dry intrusion that appeared to be responsible for the multiplicity of rainbands. The existence of such periodicity might lead one to suspect inertio-gravity waves (so-called mesoscale gravity waves). The fact that their epicentre was at the exit of a 300 hPa jet in excess of 60ms^{-1} would be consistent with this. According to Uccellini and Koch (1987) inertio- gravity waves tend to be triggered in such regions as part of the geostrophic adjustment process. However, the absence of corresponding mesoscale surface pressure perturbations greater than 0.5 hPa argues against, but perhaps does not rule out, this interpretation. One of the factors that enables inertio-gravity waves to be sustained is the existence of a statically stable layer beneath the level where the waves are triggered (Lindzen and Tung 1976). The absence of a major stable layer (such as the warm frontal zone) in the warm-sector region where the rainbands were strongest also argues against the inertio-gravity wave hypotheses: on the other hand, as shown in Fig. 11, there were shallower stable layers at the base of the dry intrusion (perhaps occasionally enhanced by melting as in Fig. 11), which may have been sufficient to sustain weak gravity waves.

An alternative hypothesis to account for the rainbands is conditional symmetric instability (CSI) (Bennetts and Hoskins, 1979). Figure 7 shows that there was a region of intense slantwise convective available potential energy (SCAPE) at the western (upwind) boundary of the arc rainbands. The SCAPE has been calculated using a method based on Shutts (1990).Release of CSI in this region would have led to the development of interleaved moist high-θ_w layers near the top of the boundary layer (as in Fig.16 of Browning et al, 1995). These would then have been advected eastwards but because they would have been in a vertically sheared flow there would have been a tendency for the slope of the interleaving layers to reverse, giving rise to that drawn in Fig.10(a). When these layers encountered a region of large-scale ascent, the potential instability implied by the interleaving layers would tend to be released, giving rise to convective bands. The convective bands would have acquired the observed arc shape as a result of the flow relative to the mesoscale vortex being cyclonic around the perimeter of the vortex (Fig.8). This explanation cannot be confirmed with the available data and is highly speculative, particularly in view of the coexistence of CAPE with SCAPE. The resolution (especially the vertical resolution) of the operational mesoscale model used in this study is insufficient to resolve CSI and this might account for its failure to represent individual arc rainbands and the fine-scale θ_w- structure at low levels. To address this issue properly future models will have to use a vertical grid spacing of order 200m (Persson and Warner 1993).

An underlying message in this study, then, is that the existing data rates for thermodynamic observations and the resolution of operational (even so-called mesoscale) models are inadequate to represent explicitly the organised mesoscale structures responsible for some coherent, long-lived, hazardous wind systems. We have been able to infer some aspects of these structures but many questions remain. In the future better resolution, and hence better understanding and predictive capability, can be achieved from increased use of ground-based remote-sensing systems and higher-resolution, non-hydrostatic, mesoscale models.

Acknowledgments

We are grateful to Peter Panagi, Ed Dicks, Richard Dixon and Gavin Winter for their parts in accessing and processing the Unified Model data, to the radiosonde teams who launched large numbers of extra sondes during the FASTEX project, to Peter Collins for coordinating the acquisition of autographic records from many Met Office observing stations and to Tim Oakley for providing the data from the Camborne Met Office UHF radar at higher-than-usual (10-minute) resolution.

References

Bader, M.J., Forbes, G.S., Grant, J.R., Lilly, R.B.E. and Waters, A.J. (Eds). 1995 Images in weather forecasting. Cambridge University Press.

Bennetts, D.A. and Hoskins, B.J. 1979 Conditional symmetric instability – a possible explanation of frontal rainbands, *Q.J.R.Meteorol.Soc.*, **105**, 945-962.

Browning, K.A. 1997 The dry intrusion perspective of extra-tropical cyclone development, *Met.Apps.*, **4,** 317-324.

Browning K.A., Ballard, S.P. and Davitt, C.S.A. 1997 High-resolution analysis of frontal fracture. *Mon.Wea.Rev.*, **125**, 1212-1230.

Browning, K.A., Clough, S.A., Davitt, C.S.A., Roberts, N.M., Hewson, T.D. and Healey, P.G.W. 1995 Observations of the mesoscale sub-structure in the cold air of a developing frontal cyclone. *Q.J.R.Meteorol.Soc.*,**121,** 1229-1254.

Browning, K.A. and Monk, G.A. 1982 A simple model for the synoptic analysis of cold fronts. *Q.J.R.Meteorol.Soc.* **108,** 435-452

Carr, F.H. and Millard, J.P. 1985 A composite study of comma clouds and their association with severe weather over the Great Plains, *Mon.Wea.Rev.*, **113**, 370-387.

Cullen, M.J.P., 1993 The unified forecast/climate model, *Meteorol.Mag, 122,* **122,** 81-94.

Fujita, T.T., 1978 Manual of downburst identification for Project NIMROD. SMRP Res. Pap.156, University of Chicago, 104pp. [NTIS PB-286048]

Gage, K.S., Williams, C.R. and Ecklund, W.L. 1994 UHF wind profilers: a new tool for diagnosing tropical convective cloud systems. *Bull.Amer.Meteorol.Soc.*, **75,** 2289-2294

Joly, A., Jorgensen, D., Shapiro, M.A., Thorpe, A.J., Bessemoulin, P., Browning, K.A., Cammas, J-P., Chalon, J-P., Clough, S.A., Emanuel, K.A., Eymard, L., Gall, R., Hildebrand, P.H., Langland, R.H., Lemaître, Y., Lynch, P., Moore, J.A., Persson, P. Ola G., Snyder., C. and Wakimoto, R.M. 1997 The Fronts and Atlantic Storm-Track Experiment (FASTEX).: Scientific objectives and experimental design *Bull.Amer.Meteorol.Soc.*, **78**,1917-1940.

Lindzen, R.S. and Tung, K.K. 1976 Banded convective activity and ducted gravity waves. *Mon.Wea.Rev.*,**104,** 1602-1617

Locatelli, J.D., Stoelinga, M.T., Schwartz, R.D and Hobbs, P.V. 1997 Surface convergence induced by cold fronts aloft and prefrontal surges, *Mon.Wea.Rev.*, **125,** 2808-2820.

Kreitzberg, C.W. 1968 The mesoscale wind field in an occlusion, *J.Appl.Meteorol.*, **7,** 53-67

Persson, P.O.G. and Warner, T.T. 1993 Nonlinear hydrostatic conditional symmetric instability : implications for numerical weather prediction, *Mon.Wea.Rev.*, **121,** 1821-1833.

Powers, J.G. and Reed, R.J. 1993 Numerical simulation of the large-amplitude mesoscale gravity-wave event of 15 December 1987 in the central United States. *Mon.Wea.Rev.*, **121,** 2285-2308.

Shutts, G.J. 1990 SCAPE charts from numerical weather prediction fields, *Mon.Wea.Rev.*, **118**, 2745-2751.

Trexler, C.M., Koch, S.E. and Ralph, F.M. 1997 Observational analysis of a mesoscale gravity wave detected during STORM-FEST. In Preprint Vol. 7th Conference on Mesoscale Processes, Reading, U.K., Amer. Meteorol.Soc., Boston, Mass. pp 559-561.

Uccellini, L.W., and Koch, S.E. 1987. The synoptic setting and possible source mechanisms for mesoscale gravity wave events. *Mon.Wea.Rev.*, **115,** 721-729.

Young, M.V., Monk, G.A. and Browning, K.A. 1987 Interpretation of satellite imagery of a rapidly deepening cyclone *Q.J.R. Meteorol. Soc.*, **113**, 1089-1115.

CURRENT JCMM INTERNAL REPORTS

This series of JCMM Internal Reports, initiated in 1993, contains unpublished reports and also versions of articles submitted for publication. The complete set of Internal Reports is available from the National Meteorological Library on loan, if required.

1. **Research strategy and programme**
   K A Browning et al
   January 1993

2. **The GEWEX Cloud System Study (GCSS)**
   GEWEX Cloud System Science Team
   January 1993

3. **Evolution of a mesoscale upper tropospheric vorticity maximum and comma cloud from a cloud-free two dimensional potential vorticity anomaly**
   K A Browning
   January 1993

4. **The global energy and water cycle**
   K A Browning
   July 1993

5. **Structure of a midlatitude cyclone before occlusion**
   K A Browning and N Roberts
   July 1993

6. **Developments in systems and tools for weather forecasting**
   K A Browning and G Szejwach
   July 1993

7. **Diagnostic study of a narrow cold frontal rainband and severe winds associated with a stratospheric intrusion**
   K A Browning and R Reynolds
   August 1993

8. **Survey of perceived priority issues in the parametrizations of cloud-related processes in GCMs**
   K A Browning
   September 1993

9. **The effect of rain on longwave radiation**
   I Dharssi
   September 1993

10. **Cloud microphysical processes - a description of the parametrization used in the large eddy model**
    H Swann
    October 1993

11. **An appreciation of the meteorological research of Ernst Kleinschmidt**
    A J Thorpe
    May 1992

12. **Potential vorticity of flow along the Alps**
    A J Thorpe, H Volkert and Dietrich Heimann
    August 1992

13. **The representation of fronts**
    A J Thorpe
    January 1993

14. **A parametrization scheme for symmetric instability: test for an idealised flow**
C S Chan and A J Thorpe
February 1993

15. **The Fronts 92 Experiment: a Quicklook Atlas**
Edited by T D Hewson
November 1993

16. **Frontal wave stability during moist deformation frontogenesis**
Part 1: Linear wave dynamics
C H Bishop and A J Thorpe
May 1993

17. **Frontal wave stability during moist deformation frontogenesis**
Part 2. The suppression of non-linear wave development
C H Bishop and A J Thorpe
May 1993

18. **Gravity waves in sheared ducts**
S Monserrat and A J Thorpe
October 1993

19. **Potential vorticity and the electrostatics analogy: quasi-geostrophic theory**
C Bishop and A J Thorpe
November 1993

20. **Recent advances in the measurement of precipitation by radar**
A J Illingworth
April 1993

21. **Micro-physique et givrage: cloud microphysics and aircraft icing**
A J Illingworth
May 1993

22. **Differential phase measurements of precipitation**
M Blackman and A J Illingworth
May 1993

23. **Estimation of effective radius of cloud particles from the radar reflectivity**
N I Fox and A J Illingworth
May 1993

24. **A simple method of Dopplerising a pulsed magnetron radar**
A Hua, A J Illingworth and J Eastment
November 1993

25. **Radiation and polar lows**
George C Craig
February 1994

26. **Collected preprints submitted to the International Symposium on the Life Cycles of Extratropical Cyclones; Bergen, Norway, 27 June - 1 July 1994**
April 1994

27. **Convective frontogenesis**
Douglas J Parker and Alan J Thorpe
April 1994

28. **Improved measurement of the ice water content in cirrus using a total water evaporator**
Philip R A Brown and Peter N Francis
April 1994

29. **Mesoscale effects of a dry intrusion within a vigorous cyclone**
K A Browning and B W Golding
April 1994

30. **GEWEX Cloud System Study, Science Plan**
May 1994

31. **Parametrization of momentum transport by convectively generated gravity waves**
R Kershaw
May 1994

32. **Mesoscale Modelling Newsletter No 5**
May 1994

33. **Observations of the mesoscale sub-structure in the cold air of a developing frontal cyclone**
K A Browning, S A Clough, C S A Davitt, N M Roberts and T D Hewson
May 1994

34. **Longwave radiative forcing of a simulated tropical squall line**
Imtiaz Dharssi
July 1994

35. **On the nature of the convective circulation at a kata-cold front**
K A Browning
September 1994

36. **Collective preprints of papers submitted to the COST-75 International Seminar on Advanced Weather Radar Systems, Brussels, 20-23 September 1994**
November 1994

37. **Use of satellite imagery to diagnose events leading to frontal thunderstorms: Parts I and II of a case study**
K A Browning and N M Roberts
November 1994

38. **The role of spaceborne millimetre-wave radar in the global monitoring of ice cloud**
P R A Brown, A J Illingworth, A J Heymsfield, G M McFarquhar, K A Browning and M Gosset
December 1994

39. **Potential vorticity inversion**
Michal Ziemianski
October 1994

40. **Theory of mature tropical cyclones; a comparison between Kleinschmidt (1951) and Emanuel (1986)**
Suzanne L Gray
December 1994

41. **Dispersion and removal of pollutants during the passage of an atmospheric frontal system**
N R Gimson
December 1994

42. **The role of snow sublimation in frontogenesis**
D J Parker and A J Thorpe
December 1994

43. **Potential vorticity and the electrostatics Analogy: Ertel-Rossby formulation**
A J Thorpe and C H Bishop
December 1994

44. **Mesoscale aspect of extratropical cyclones: an observational perspective**
K A Browning
January 1995

45. **A polar low outbreak: evolution and mesoscale structures**
T D Hewson, G C Craig and C Claud
February 1995

46. **Generation of near-surface gusts of deep convection**
K Nakamura and R Kershaw
April 1995

47. **Attribution concepts applied to the Omega Equation**
S A Clough, C S A Davitt and A J Thorpe
June 1995

48. **Parametrization of mixed-phase cloud and precipitation**
Susan P Ballard and M Gerard Hutchinson
June 1995

49. **Short-range forecasting of stratocumulus: initialization prediction**
Susan P Ballard, Simon D Jackson and B Macpherson
June 1995

50. **Contributions of the JCMM/Dept of Meteorology Radar Group to the 27th AMS Radar Meteorology Conference, Vail October 1995**
June 1995

51. **Cold pools in shear**
Douglas J Parker
September 1995

52. **High-resolution analysis of frontal fracture**
K A Browning, S P Ballard and C S A Davitt
September 1995

53. **The albedo of broken cloud fields: calculations using a modified two stream radiation code**
Imtiaz Dharssi and Roy Kershaw
October 1995

54. **Parametrization of momentum transport by convection. I: theory and cloud modelling results**
R Kershaw and D Gregory
November 1995

55. **Variation of frontal structure along a cold front**
K A Browning and N M Roberts
November 1995

56. **Secondary frontal waves**
Douglas Parker
December 1995

57. **Objective fronts**
T D Hewson
March 1996

58. **Mesoscale analysis of the activation of a cold front during cyclogenesis**
K A Browning, N M Roberts and A J Illingworth
June 1996

59. **Investigation of different representations of rain in a 1-d evaporation model**
H Swann
May 1996

60. **Parametrization of diabatic processes in the inversion of the omega-equation**
M Athanassiadou and A J Thorpe
June 1996

61. **The role of the environmental flow in the development of secondary frontal cyclones**
I A Renfrew, A J Thorpe and A Joly
June 1996

62. **Consequences of the geostrophic momentum approximation on barotropic instability**
S Malardel, A J Thorpe and A Joly
June 1996

63. **Contributions to the AMS/RMS Conference on Mesoscale Processes**
Reading, 9-13 September 1996

64. **Vorticity and potential vorticity in stratified flows interacting with an isolated obstacle**
Jorge A Gutiérrez and A J Thorpe
September 1996

65. **Triple point development: two case studies**
Douglas Parker
September 1996

66. **Radar observations of wind-shear splitting within evolving atmospheric Kelvin-Helmholtz billows**
D Chapman and K A Browning
April 1997

67. **Cold frontal structure derived from radar wind profilers**
K A Browning, D Jerrett, J Nash, T Oakley and N M Roberts
May 1997

68. **The dry intrusion and its effect on the frontal, cloud and precipitation structure of extratropical cyclones**
K A Browning - Text of invited special lecture at the Spring Conference
of the Meteorological Society of Japan, University of Tsukuba, 22 May 1997

69. **Met. Office Unified Model data, diagnostics, graphics programs, and other observational data available from the JCMM through the aegis of the Universities Weather Research Network (UWERN).** (Plus supplement)
Peter Panagi and Ed Dicks
June 1997

70. **Contributions of the JCMM/Dept of Meteorology Radar Group to the 28th AMS Radar Meteorology Conference.** Austin, Texas
September 1997

71. **Sensitivity of short-range weather forecasts to local potential vorticity modifications**
Meral Demirtas and Alan Thorpe
July 1997

72. **Objective identification of frontal wave cyclones**
T D Hewson
August 1997

73. **Attribution and its application to mesoscale structure associated with tropopause folds**
A J Thorpe
September 1997

74. **The role of the environmental flow in the development of secondary frontal cyclones**
Ian A Renfrew, Alan J Thorpe and Craig H Bishop
September 1997

75. **Potential vorticity: a short history of its definitions and uses**
Alan J Thorpe and Hans Volkert
September 1997

76. **Superposing semi-geostrophic potential vorticity anomalies**
H R Birkett and A J Thorpe
September 1997

77. **Short period forecasting of catchment-scale precipitation.**
Part 1: the role of Numerical Weather Prediction
M A Pedder, M Haile and A J Thorpe
September 1997

78. **Verification of the tracking technique used in an experimental cloud motion wind inferring system**
Z Wang, K A Browning and G A Kelly
October 1997

79. **A preliminary study of Fourier series analysis for cloud tracking with GOES high temporal resolution images**
Z Wang
October 1997

80. **Analysis of an ex-tropical cyclone after reintensifying as a warm-core extratropical cyclone**
K A Browning, G Vaughan and P Panagi
November 1997

81. **A JCMM overview of FASTEX IOPs**
S A Clough, H W Lean, N M Roberts, H Birkett, J-P Chaboureau, R Dixon, M Griffiths, T D Hewson and A Montani
January 1998

82. **Programs for PV inversion and modification**
Meral Demirtas
December 1997

83. **Release of potential shearing instability in warm frontal zones**
D Chapman and K A Browning
February 1998

84. **The European Cloud-Resolving Modelling Programme (EUCREM)**
Summary Report from the coordinator
P W White
April 1998

85. **A frontal wave database**
T D Hewson
April 1998

86. **Layering observed in dropsoundings from IOP 1 of Fronts 92**
S A Clough
May 1998

87. **Use of wind-shear displays for Doppler radar data**
D Chapman and K A Browning
May 1998

88. **Radar estimates of rainfall rates at the ground in bright band and non-bright band events**
T J Smyth and A J Illingworth
June 1998

89. **Correction for attenuation of radar reflectivity using polarisation data**
T J Smyth and A J Illingworth
June 1998

90. **The effects of convection on chemical reactions and precipitation scavenging**
Neil R Gimson
July 1998

91. **How to use the display program DISP**
Nigel Roberts
August 1998

92. **Conceptual models of cyclogenesis**
Adrian T Semple
August 1998

93. **Observations of oblate hail using dual polarisation radar and implications for hail detection schemes**
T J Smyth, T M Blackman and A J Illingworth
September 1998

94. **The semigeostrophic diagnosis of vertical motion. Part I: Formulation and co-ordinate transformations**
Mike A Pedder and Alan J Thorpe
September 1998

95. **The semigeostrophic diagnosis of vertical motion. Part II: Results for an idealised baroclinic wave life cycle**
Alan J Thorpe and Mike A Pedder
September 1998

96. **Convective destabilisation by a tropopause fold diagnosed using potential vorticity inversion**
Morwenna Griffiths, Alan Thorpe and Keith Browning
October 1998

97. **Forecast skill of the ECMWF model using targeted observations during FASTEX**
A Montani, A J Thorpe, R Buizza and P Unden
October 1998

98. **Observations and model simulations of the FASTEX IOP 16 frontal wave - effects of sublimation**
Sid A Clough, Humphrey W Lean, Nigel M Roberts and Richard M Forbes
December 1998

99. **The application of conceptual models in NWP**
Adrian T Semple
January 1999

100. **Mesoscale analysis of arc rainbands in a dry slot**
K A Browning and N M Roberts
January 1999

Met Office Joint Centre for Mesoscale Meteorology Department of Meteorology
University of Reading PO Box 243 Reading RG6 6BB United Kingdom
Tel: +44 (0)118 931 8425 Fax: +44 (0)118 931 8791
www.metoffice.com